Supplementary Information (SI) for Environmental Science: Nano.
This journal is © The Royal Society of Chemistry 2026

Supplementary Information for:

High-content imaging reveals how tuning nanoparticle hydrophobicity impacts interactions between porous silica nanoparticles and plant biosurfaces

Eric Ostovich[1*], Cheng-Hsin Huang[2], Lissett G. Diaz[3], Christy L. Haynes[2], Rebecca Klaper[1,3]

[1,3]School of Freshwater Sciences, University of Wisconsin-Milwaukee, Milwaukee, WI, USA

[2]Department of Chemistry, University of Minnesota-Twin Cities, Minneapolis, MN, USA

Pages: 14

Tables: 1

Figures: 13

Contact angle measurement. Since direct measurement of nanoparticle hydrophobicity is challenging,[1,2] glass slides were coated with TMS and PEG at the same ratios used in nanoparticle synthesis to approximate the nanoparticle surfaces. Water contact angle measurements on the coated slides were used to estimate the relative surface hydrophobicity. Coating of the glass slides were performed based on a published protocol[3] with some modifications. Briefly, solutions with 3 to 5 % water in ethanol (v/v) were prepared, and the pH was adjusted to 4.5 to 5.5 with acetic acid. Different mole ratios (1:1, 1:2, 1:3) of TMS and PEG were added to the mixtures to reach a total silane concentration of 3% (v/v). The mixtures were stirred at room temperature for 5 min to allow the formation of reactive silanols. The glass slides were then in contact with the stirring mixture for 2 hours. After that, the coated glass slides were washed several times with ethanol to remove the excess silanes followed by incubation in an oven at 110 °C for 30 minutes.

A drop of water was added to each glass slide, and the contact angles formed between the water droplets and the glass slides were measured by MCA-3 automatic microscopic contact angle meter (Kyowa Interface Science Co., Japan). For each measurement, 30 images were captured within 1392 ms following the contact of the water drop with the glass slide, and contact angles were measured from each image. All measurements were performed in triplicate, and the contact angles reported in **Table S1** represent the mean ± standard deviation calculated from all measurements.

Table S1. Contact angle measurements of water droplets on glass slides coated with different ratios of TMS and PEG. Reported values represent the mean ± standard

deviation calculated from 90 measurements (30 frames per replicate, 3 replicates). Representative top-view and side-view images of the water droplet on each surface are also shown. All coated samples exhibited contact angles of ~6°, indicating hydrophilicity beyond the resolution of contact angle measurements for distinguishing between them.

Slide	Top-view	Side-view	Contact angle (°)
Bare glass slide	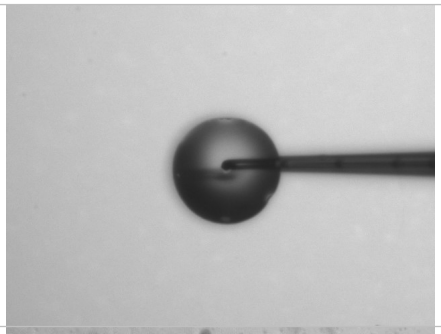	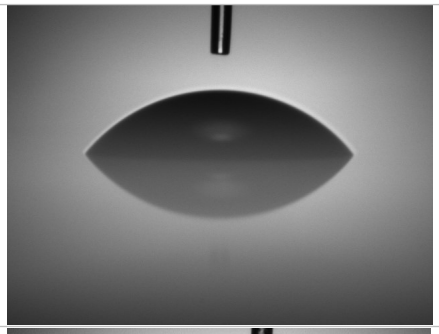	**50.5 ± 0.5**
TMS:PEG 1:1	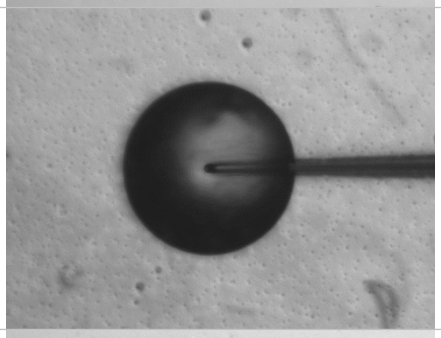	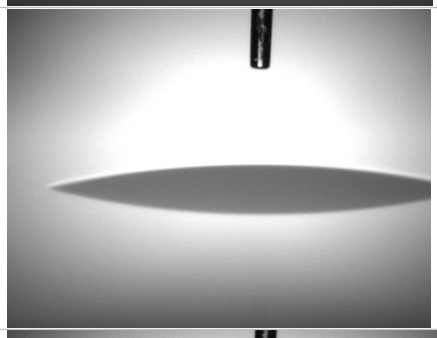	**6.8 ± 1.1**
TMS:PEG 1:2	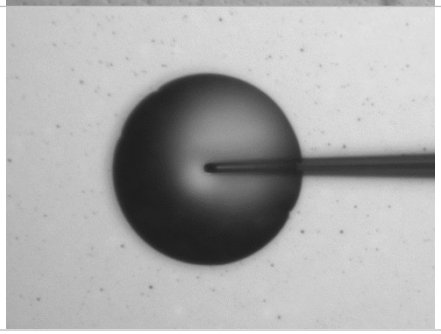	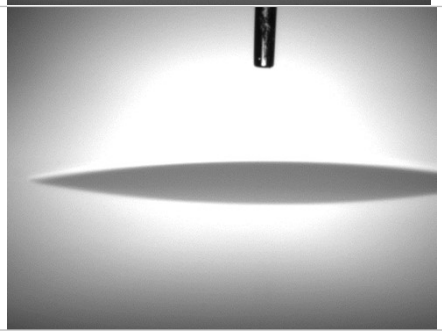	**5.6 ± 0.6**

TMS:PEG 1:3	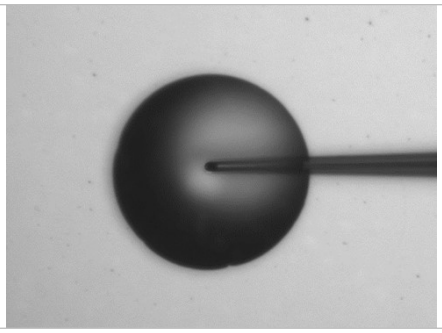	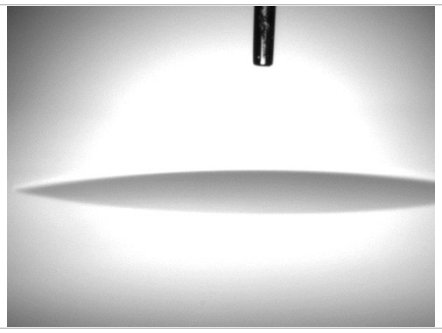	**6.8 ± 1.7**

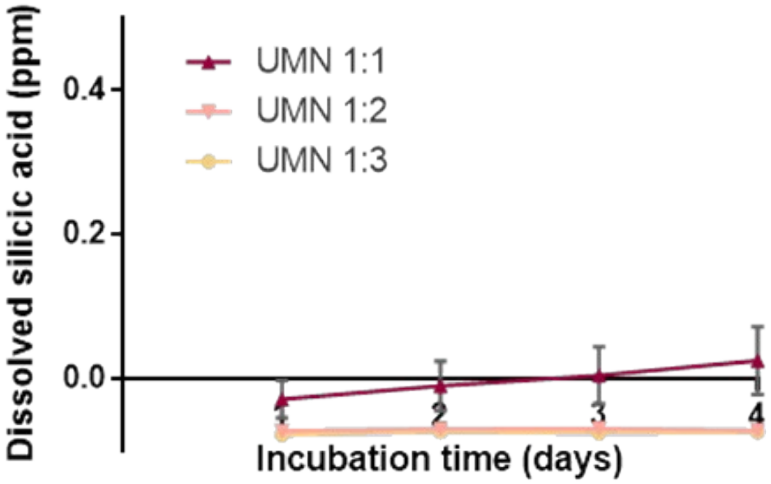

Figure S1: UMN dissolution in water over 3 days. As shown in the figure, no significant dissolution of silicic acid from the UMNs was observed within this period, indicating that the nanoparticles remained stable.

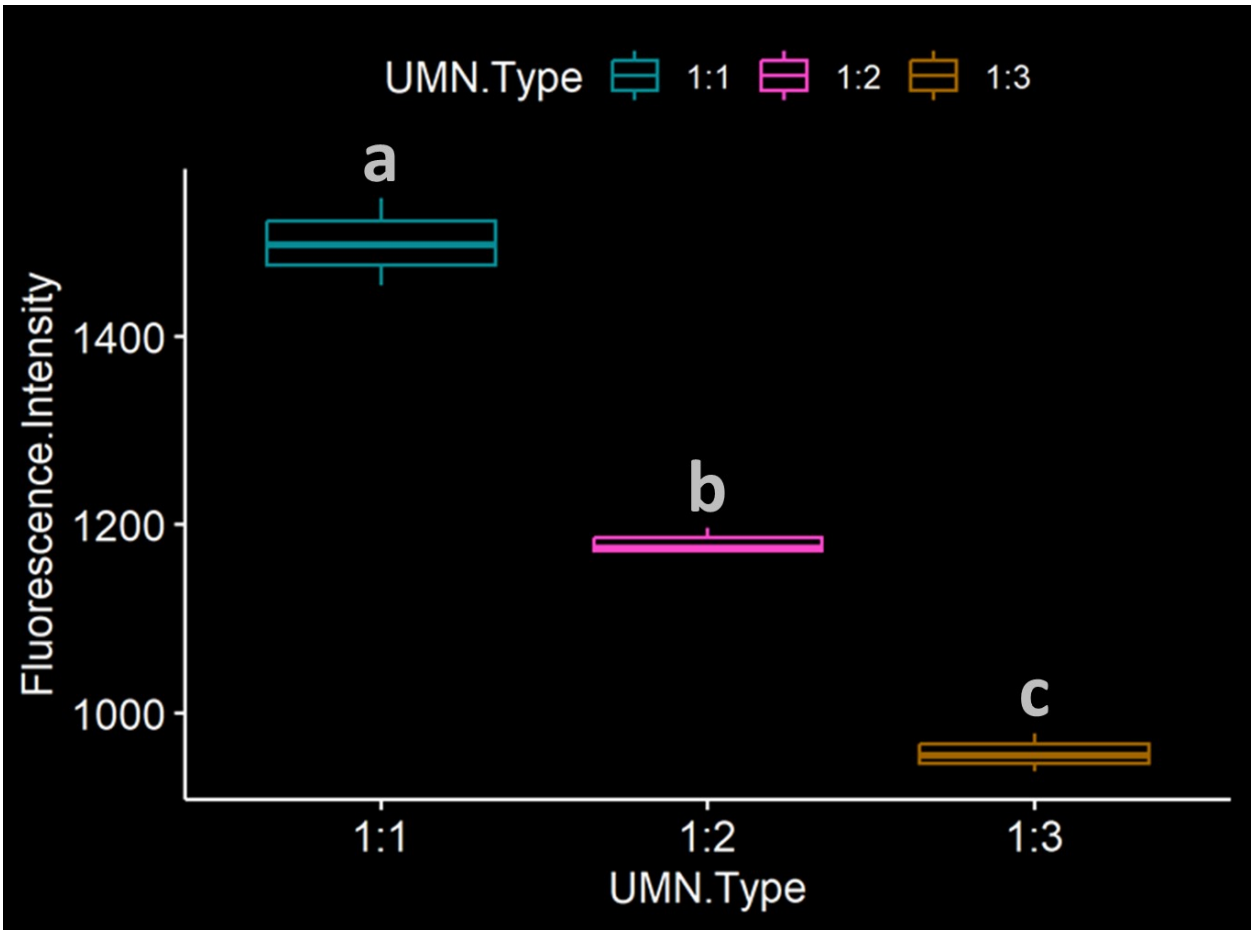

Figure S2: Relative fluorescence of UMNs at the same concentration (100 ppm). Data was collected in triplicates and significant differences were determined using a two-way ANOVA with a Tukey post hoc for multiple comparisons; columns with different letters differ significantly ($p < 0.05$).

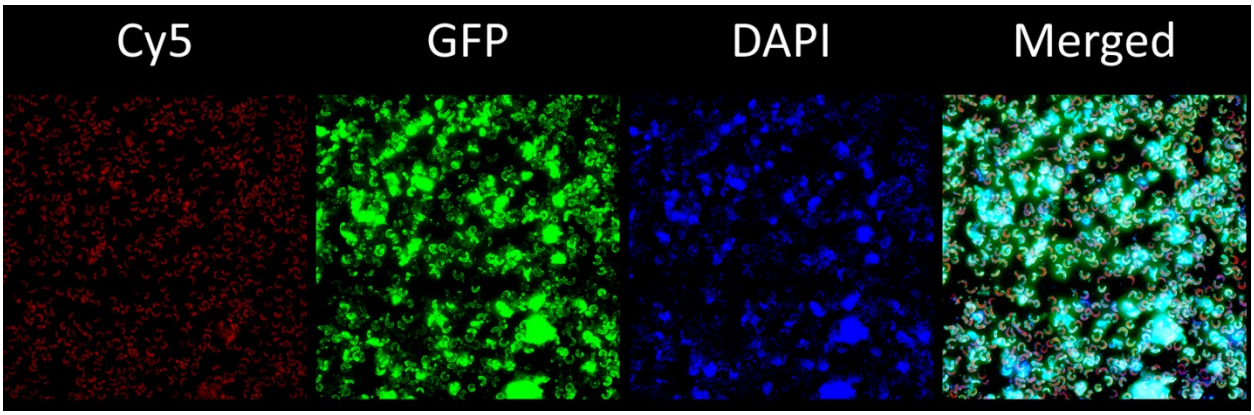

Figure S3: Separate fluorescent channels of amine-functionalized PSNPs exposed to algae at 5 ppm for 1 hour (Cy5; chloroplasts, GFP; PSNPs, DAPI, nuclear stain). Here NP's have absorbed external fluorescent dyes, making fluorescent signal uninterpretable.

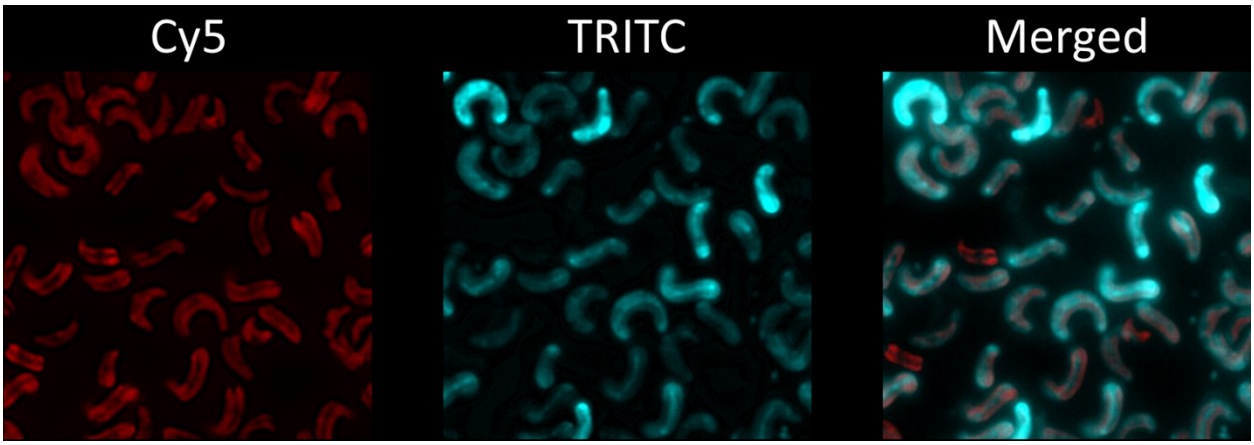

Figure S4: Algal cells dyed with Safranin-O, which binds to cellulose fibers in plants and algae to visualize the cell wall (Cy5; chloroplast, TRITC; cell wall).

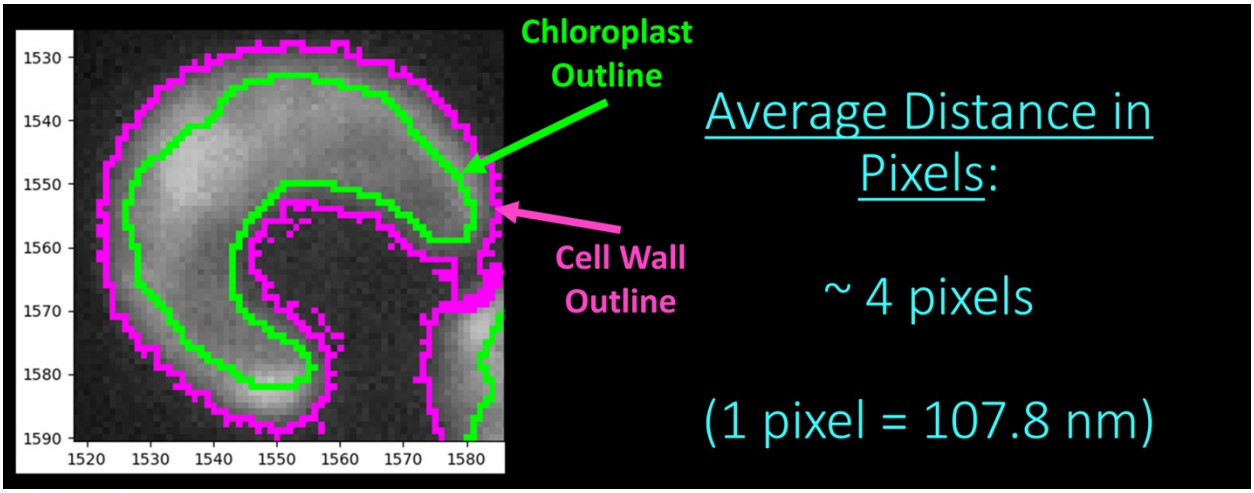

Figure S5: CellProfiler plot highlighting the chloroplast and cell wall boarders, of which CellProfiler was used to calculate the average distance in pixels between the two.

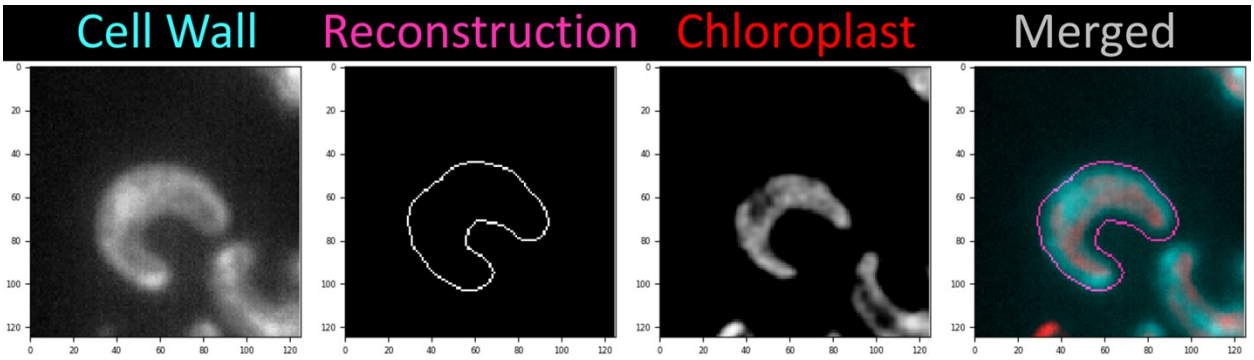

Figure S6: 2D reconstruction of the cell wall using the chloroplast as a reference point.

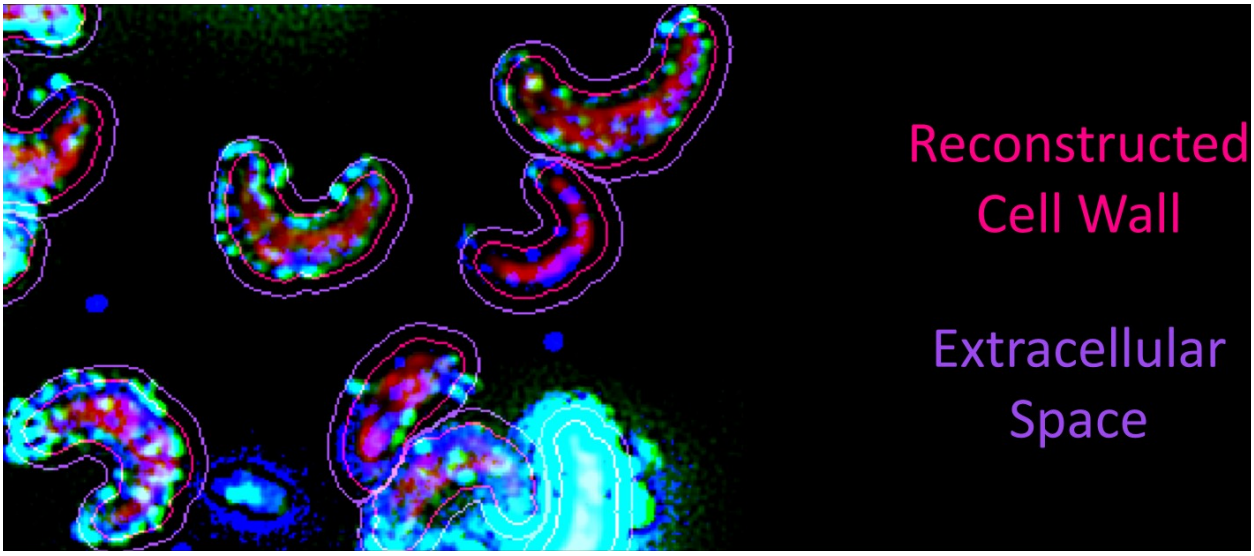

Figure S7: Cell wall reconstructed on PSNP-treated cells. Here, the addition of the reconstructed cell wall allows for the predicted quantification of internalized particles, while an additional border is added to allow for the predicted quantification of externally bound particles.

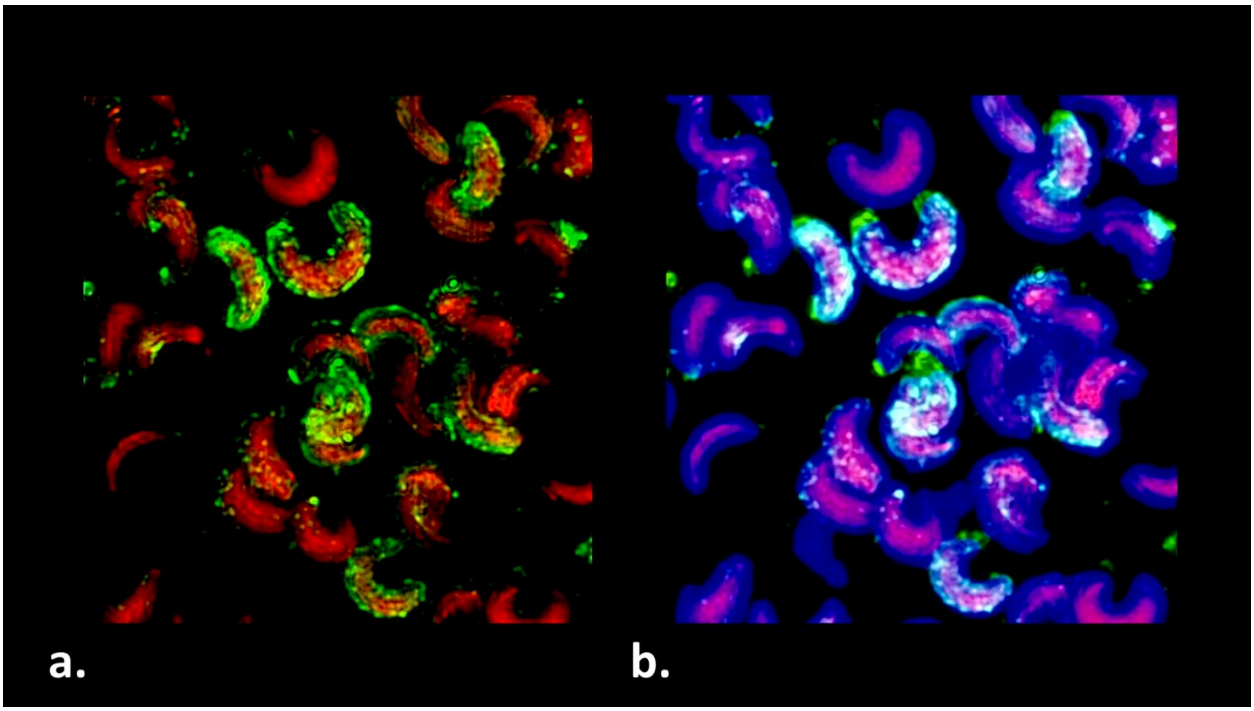

Figure S8: (a) Algae exposed to 5 ppm of amine-functionalized PSNPs for 1 hour without the addition of the reconstructed cell wall. Here the differentiation between externally adsorbed and internalized PSNPs (in green) is difficult. In some of the cells, the PSNPs appear to have a relative distance from the chloroplast border. (b) Algae exposed to 5 ppm of amine-functionalized PSNPs for 1 hour with the addition of the reconstructed cell wall. Here the differentiation between externally adsorbed PSNPs (in green) and internalized PSNPs (in cyan) is possible. In some of the cells, where the PSNPs appear to have a relative distance from the chloroplast border, the reconstructed cell wall matches up perfectly with those PSNP signals.

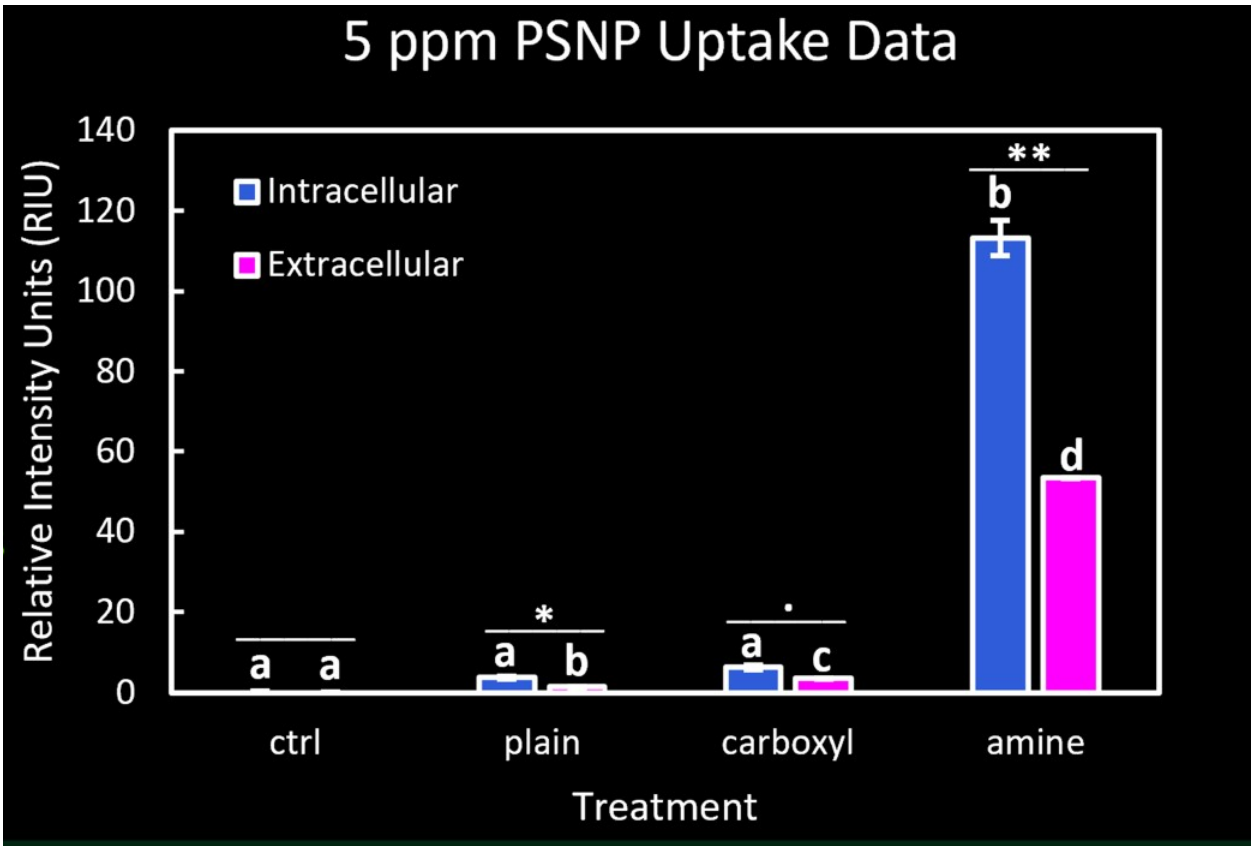

Figure S9: Relative estimated levels of PSNP uptake and absorption. Significant differences were determined using a two-way ANOVA with a Tukey post hoc for multiple comparisons; columns with different letters differ significantly ($p < 0.05$).

As a proof of concept, this method was used to estimate the levels of cellular uptake/adherence of PSNPs with different functional groups. Cells were exposed to 5 ppm of plain, carboxyl-, or amine-functionalized PSNPs, which have no charge, negative charge, and positive charge, respectively. A CellProfiler pipeline was written to quantify the relative levels of PSNP uptake and adherence. PSNP presence was measured using the integrated intensity of PSNP fluorescence signal; PSNP signal within the cell wall boarder was considered as uptaken, and signal directly outside cell wall boarder was considered as adhered. PSNP fluorescence was also normalized to the control by subtracting the background GFP signal of non-treated cells from all PSNP treated cells. Based on these measurements (**Fig. S9**), significantly higher levels of interaction (both uptake and adherence) were estimated with amine-functionalized PSNPs in comparison to other functionalizations. This is likely due to the enhanced attraction of the positively-charged PSNPs to the negatively-charged cell surface. However, more interestingly, higher levels of uptake past the cell wall were estimated compared to levels of adherence outside the cell wall for all treatments, with significant differences in both the plain and amine-PSNP treatments. These results imply that PSNPs can and do pass across plant-type cell walls.

This distinction is an important one to make as it completely changes the narrative from PSNPs sticking to the outside of the cell blocking light and nutrients to PSNPs being able to physically interact with internal structures inside the cell. Overall, this simple method could be implemented for other fluorescent nanoparticle types and could be a useful tool for understanding/charactering nanoparticle interactions with plant-type biological surfaces.

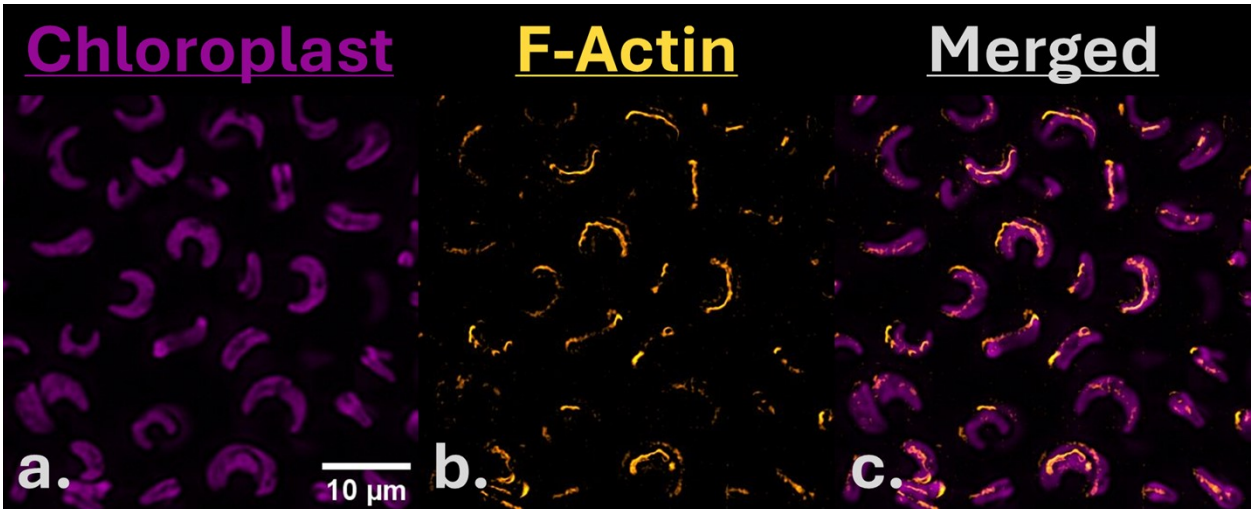

Figure S10: Staining patterns of F-actin using rhodamine phalloidin in *R. subcapitata*. Based on thes staining patterns, the general shape of the F-actin (without the presence of UMNs) appears to be very similar to that of the F-actin in the phalloidin-stained cells (in the presence of UMNs) in the main text (**Fig 5a**). This provides some confidence that the phalloidin dye is binding to the F-actin, rather than the UMNs itself.

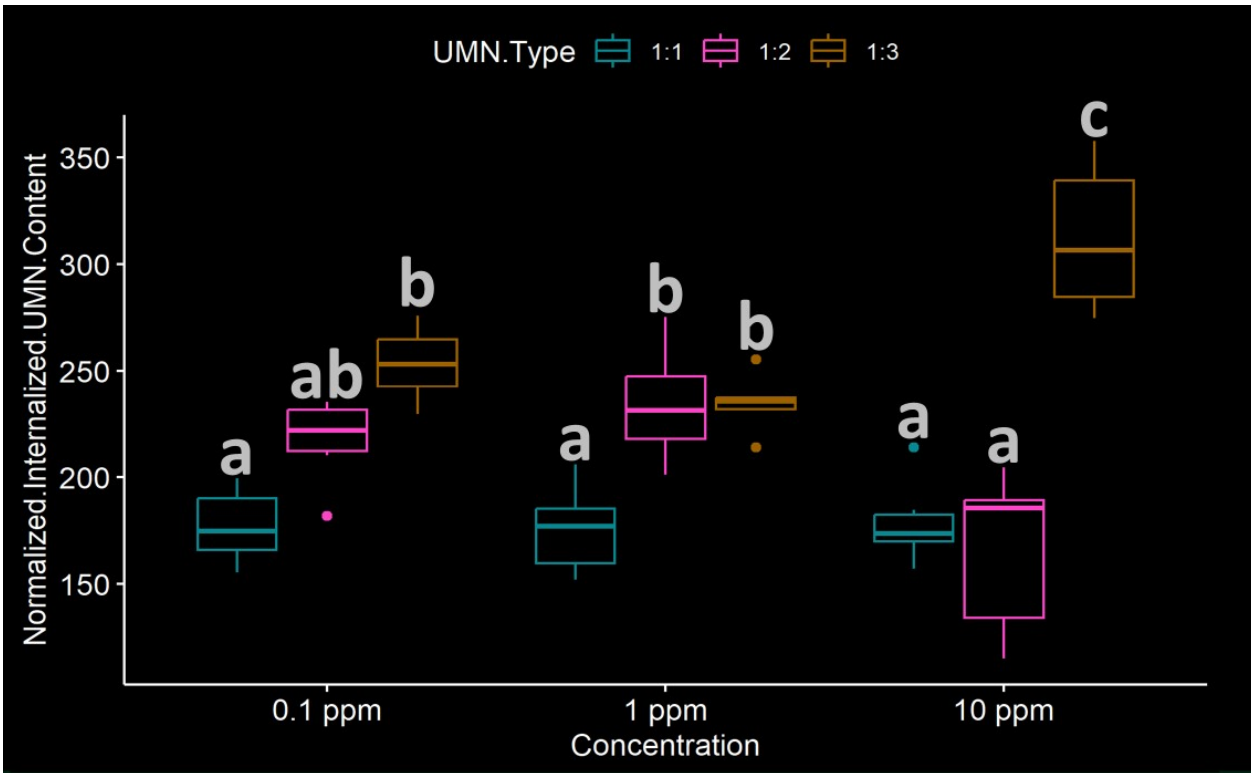

Figure S11: Internalization of UMNs after 24 hours. Here, normalized fluorescence signals represent relative levels of internalized UMN content across concentration and particle type. Significant differences were determined using a two-way ANOVA with a Tukey post hoc for multiple comparisons; columns with different letters differ significantly ($p < 0.05$).

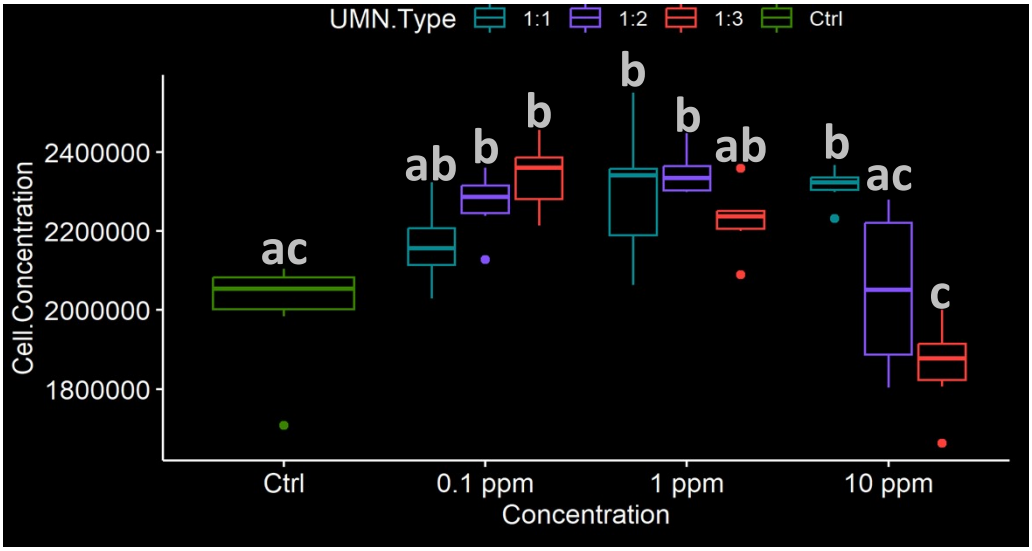

Figure S12: Concentration of cells after 24 hours of exposure to UMNs. Significant differences were determined using a two-way ANOVA with a Tukey post hoc for multiple comparisons; columns with different letters differ significantly ($p < 0.05$).

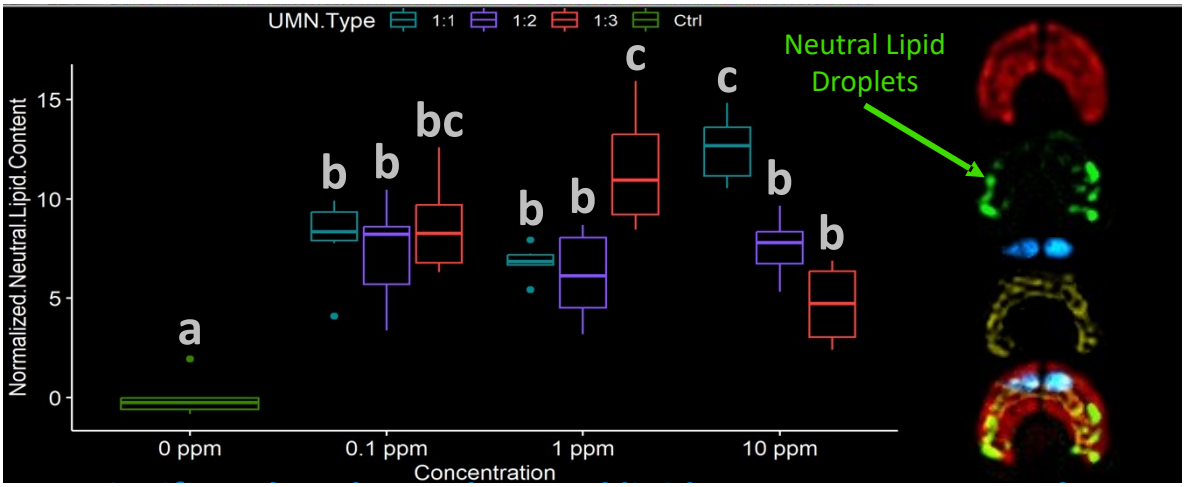

Figure S13: Relative neutral lipid droplet content in UMN-exposed algae after 24 hours. Significant differences were determined using a two-way ANOVA with a Tukey post hoc for multiple comparisons; columns with different letters differ significantly ($p < 0.05$).

Justification for Using *R. subcapitata* as an in vitro model for plant-type cells.

R. subcapitata was a strategic choice for modeling these interactions, compared to protoplasts and/or isolated plant tissues, for several reasons. First, while protoplasts and isolated plant tissues offer the advantage of representing the highest similarity and natural complexity to their parent tissue/organism counterparts, they tend to be fragile (particularly when missing a cell wall), and their preparation and maintenance can be time-consuming and challenging, thus posing difficulties in achieving consistent imaging, especially for high-throughput applications.[4,5,6] By comparison, *R. subcapitata* cells are sturdy, robust, and relatively easy to grow and maintain in controlled laboratory conditions. Additionally, as a monoculture that does not form colonies or coenobia under stress, they can be grown in morphologically uniform populations, thereby reducing cell-

to-cell variability and offering more reproducible results for high-content imaging-based studies.[7,8] This type of cell homogeneity, by contrast, can be difficult to achieve with protoplasts and isolated plant tissue, where the heterogeneity of their cells (both morphologically and by cell type, respectfully) can introduce more cell-to-cell variability, complicating high-content imaging and downstream bioimage segmentations.[9,10,11] Furthermore, despite not fully replicating the complexity of higher plants, *R. subcapitata* cells still share many similarities with the mesophyll cells of higher plants, such as rigid cell wall structures with high cellulose content, similar subcellular compartments, and the evolutionarily conserved pathways and environmental processes that they both carry out.[12,13,14] Lastly, *R. subcapitata*, in combination with MACI, has been proven to offer a quick and effective framework for characterizing complex phenotypes and for investigating cellular targets in plant-type organisms, making this system ideal for visualizing nanoparticle interactions and their translocation within the cell.[15,16]

References:

1. Li, G., Cao, Z., Ho, K. K. H. Y. & Zuo, Y. Y. Quantitative Determination of the Hydrophobicity of Nanoparticles. *Anal. Chem.* **94**, 2078–2086 (2022).
2. Crandon, L. E., Boenisch, K. M., Harper, B. J. & Harper, S. L. Adaptive methodology to determine hydrophobicity of nanomaterials in situ. *PLoS One* **15**, 1–17 (2020).
3. Borup, B. & Weissenbach, K. *Silane Coupling Agents*. *Bioconjugate Techniques, Third Edition.* (2013). doi:http://dx.doi.org/10.1016/B978-0-12-382239-0.00013-3 535
4. Li, X. *et al.* Efficient Protoplast Regeneration Protocol and CRISPR/Cas9-Mediated Editing of Glucosinolate Transporter (GTR) Genes in Rapeseed

(Brassica napus L.). *Front. Plant Sci.* **12**, 1–11 (2021).

5. Monthony, A. S. & Jones, A. M. P. Enhancing Protoplast Isolation and Early Cell Division from Cannabis sativa Callus Cultures via Phenylpropanoid Inhibition. *Plants* **13**, 1–14 (2024).

6. Yoo, S. D., Cho, Y. H. & Sheen, J. Arabidopsis mesophyll protoplasts: A versatile cell system for transient gene expression analysis. *Nat. Protoc.* **2**, 1565–1572 (2007).

7. Zachleder, V., Bišová, K. & Vítová, M. *The Physiology of Microalgae*. *The Physiology of Microalgae* (Springer, Cham, 2016). doi:10.1007/978-3-319-24945-2

8. Roccuzzo, S. *et al.* Metabolic Insights Into Infochemicals Induced Colony Formation and Flocculation in Scenedesmus subspicatus Unraveled by Quantitative Proteomics. *Front. Microbiol.* **11**, 1–17 (2020).

9. Dawson, J. *et al.* Determination of protoplast growth properties using quantitative single-cell tracking analysis. *Plant Methods* **18**, 1–15 (2022).

10. Hafke, J. B., Furch, A. C. U., Reitz, M. U. & Van Bel, A. J. E. Functional sieve element protoplasts. *Plant Physiol.* **145**, 703–711 (2007).

11. Pasternak, T., Lystvan, K., Betekhtin, A. & Hasterok, R. From single cell to plants: Mesophyll protoplasts as a versatile system for investigating plant cell reprogramming. *Int. J. Mol. Sci.* **21**, 1–15 (2020).

12. Machado, M. D. & Soares, E. V. Features of the microalga Raphidocelis subcapitata : physiology and applications. *Appl. Microbiol. Biotechnol.* (2024). doi:10.1007/s00253-024-13038-0

13. Lu, Y. & Xu, J. Phytohormones in microalgae: A new opportunity for microalgal biotechnology? *Trends Plant Sci.* **20**, 273–282 (2015).

14. Riaz, A. *et al.* Molecular Regulation and Evolution of Redox Homeostasis in Photosynthetic Machinery. *Antioxidants* **11**, 1–23 (2022).

15. Ostovich, E. & Klaper, R. Using a novel multiplexed algal cytological imaging (MACI) assay and machine learning as a way to characterize complex phenotypes in plant-type organisms. *Environ. Sci. Technol.* **58**, 4894–4903 (2024).

16. Ostovich, E., Henke, A., Green, C. & Klaper, R. Predicting the phytotoxic mechanism of action of LiCoO2 nanomaterials using a novel multiplexed algal cytological imaging (MACI) assay and machine learning. *Environ. Sci. Nano* **11**, 507–517 (2024).